

Scattering of surface plasmon-polaritons in a graphene multilayer photonic crystal with inhomogeneous doping

Yu. V. Bludov, N. M. R. Peres, G. Smirnov, M. I. Vasilevskii

Department of Physics and Center of Physics, University of Minho, P-4710-057, Braga, Portugal

The propagation of a surface plasmon-polariton along a stack of doped graphene sheets is considered. This auxiliary problem is used to discuss: (i) the scattering of such a mode at an interface between the stack and the vacuum; (ii) the scattering at an interface where there is a sudden change of the electronic doping. The formalism is then extended to the *barrier problem*. In this system rich physics is found for the plasmonic mode, showing: total reflection, total transmission, Fabry-Pérot oscillations, and coupling to photonic modes.

PACS numbers: 81.05.ue,72.80.Vp,78.67.Wj

I. INTRODUCTION

Plasmonics deals with the excitation, manipulation, and utilization of surface plasmon-polaritons (SPPs), where the latter are hybridized excitations of radiation with the collective charge oscillations of an electron gas^{1–3}. In traditional noble-metal plasmonics the electron gas is provided by the free electrons in the metal. Furthermore, SPPs are excited at the interface between a metal and a dielectric and propagate along the interface with exponential localization in the direction perpendicular to that of their motion.

One central idea in plasmonics is to explore the sub-wavelength confinement of light to build plasmonic waveguides that would propagate, at the same time, an electric signal and a highly confined electromagnetic wave⁴. A plasmonic circuitry would involve lenses, mirrors, beam splitters, and the like. Therefore, the study of scattering of plasmons by such structures arises.

Clearly, the problem of scattering of plasmons is a scientific and technological one. The deep understanding of the scattering of plasmons is instrumental for building new technologies. In traditional noble-metal plasmonics, the range of wavelengths where SPPs show sub-wavelength confinement is restricted to the interval spanning the near infrared (near-IR) to the ultraviolet. In the mid-infrared (mid-IR) to the terahertz (THz) spectral range SPPs in structures with noble metals are essentially free radiation, therefore lacking the key advantage of sub-wavelength confinement. This makes them unsuitable for plasmonics circuitry and sensing⁵.

From what has been said above it follows that new plasmonic materials able of showing sub-wavelength confinement and spanning the frequency interval ranging from the THz to the mid-IR are necessary. This is particularly relevant as important biomolecules exhibit unique spectral signatures in this frequency range. Thus, the sensing capability arising with noble-metal plasmonics in the near-IR to the ultraviolet could be extended to a region that the traditional systems cannot cover. Such possibility would increase the application of plasmonics for sensing and security applications, such as detection of pollutants, diagnosis of diseases, food control quality,

and detection of plastic explosives.

It is in the above context that graphene emerges as a promising plasmonic material^{2,6–11}. SPPs in graphene exist in the THz to mid-IR range and show a high degree of sub-wavelength localization, therefore circumventing the mentioned limitations of noble-metal plasmonics. Indeed, it can be shown that the degree of localization of plasmons in graphene is given by¹²

$$\zeta_G \propto \alpha \hbar c \frac{E_F}{(\hbar\omega)^2}, \quad (1)$$

where α is the fine structure constant of atomic physics, c is the speed of light, E_F is the Fermi energy of graphene, and ω is the frequency of the surface plasmon-polariton. Taking, as an example, a frequency of 150 THz (equivalent to the wavelength of $\lambda_0 = 2 \mu\text{m}$ for the radiation in vacuum, which corresponds to the edge of the mid-IR region), and considering a typical Fermi energy of 0.5 eV (a value easily attainable by the electrostatic gating) we obtain for $\zeta_G \sim 0.002 \mu\text{m}$, that is

$$\frac{\lambda_0}{\zeta_G} \sim 10^3, \quad (2)$$

which is a rather high degree of localization. This value yields highly intense and localized electromagnetic fields. The above estimation highlights the potential of graphene plasmonics in the THz to mid-IR spectral range.

Being a two-dimensional membrane, graphene is amenable for stacking. The idea is to build a photonic crystal composed by several stacked sheets of graphene separated by dielectric layers; this structure has been investigated both theoretically^{7,13–23} and experimentally^{24,25}. In such structures charge carriers in different graphene layers are able to interact by means of electromagnetic waves, which can be either propagating or evanescent inside the dielectric. The latter case refers to the area of plasmonics, where interaction between the SPPs supported by each of the graphene layers results in the formation of polaritonics bands^{7,18,26,27}. This fact allows for the existence of a number of interesting phenomena such as Bloch²⁸ and Rabi²⁹ oscillations of SPPs as well as the formation of nonlinear self-localized wavepackets —lattice solitons^{30,31}. Moreover,

it was predicted that a plasmonic biosensor based on a graphene multilayer system shows a much higher sensitivity than its counterpart operating using a gold film³². The propagation of bulk waves in a graphene stack is characterized by several phenomena typical for periodic structures, like the presence of the omnidirectional low-frequency gap^{19–21} in the spectrum (which is not present in the photonic crystals without graphene), extraordinary absorption decrease²², and light pulse delay³³. In practice, these graphene multilayers can be used as terahertz modulators³⁴, broadband polarizers³⁵, tunable Bragg reflectors⁷, and polarization splitters²⁰. Also it is interesting that the graphene stacks exhibit the properties of hyperbolic metamaterials^{36–38}. Finally, the study of propagation of radiation in a disordered graphene stack when light impinges perpendicularly to the graphene surface has recently been considered¹⁷, showing that graphene can control Anderson localization of radiation.

As mentioned above, eventually it will be necessary to build some kind of plasmonic circuitry where the problem of scattering of SPPs arises. In graphene, it is possible to control the percentages of reflection and transmittance of a surface plasmon-polariton by controlling the local value of the electronic density. Consider the simplest case of a graphene sheet on a split gate. Each of the two parts of the gate is subjected to different gate potentials, and this creates two zones in the material presenting two different electronic concentrations. Assuming now that a surface plasmon-polariton is impinging on the border line defined by the split gate, the amount of power reflected and transmitted will be controlled by the difference in the local electronic densities. The problem just described has already been discussed in the literature^{39,40}. Another interesting question is the coupling of SPPs to photonic modes. The idea can work in two ways: either a photonic mode will excite a surface plasmon-polariton in graphene or a surface plasmon-polariton propagating on graphene will radiate to free space as a photonic mode. Both cases find relevant technological applications.

As we will show in the bulk of the article, it is easier to achieve the interaction between SPP and photonic modes in the graphene stack, than in single graphene layer. Due to the periodicity of the system, this interaction can be direct (i.e. without using prisms). Also the scattering of SPPs in a stack of graphene sheets has rich physics, including total reflection, total transmission, and Fabry-Pérot oscillations.

The paper is organized as follows. In Sec.II we consider the eigenvalues and the eigenfunctions of a graphene multilayer photonic crystal (PC), which will serve as a basis for the following sections. Sec.III is devoted to two problems: (i) scattering of an incident polaritonic mode at the interface between the graphene multilayer PC and a homogeneous dielectric; (ii) scattering of an incident polaritonic mode at the interface between two PCs, characterized by different Fermi energies of the graphene sheets. In Sec.IV we consider the scattering of a polaritonic mode on a double interface between PCs.

II. EIGENMODES OF THE GRAPHENE MULTILAYER PHOTONIC CRYSTAL

In order to calculate the reflection of SPPs from the interface between two graphene multilayer PCs, it is necessary to know the spectrum of the electromagnetic waves in PC. In the present section we consider an auxiliary problem of eigenmodes in a multilayer graphene stack composed of an infinite number of single graphene layers with equal Fermi energy E_F [see Fig.1(g)]. We suppose that graphene layers are arranged at equal distances d from each other at planes $z = md$, $m \in (-\infty, \infty)$ and are embedded into a uniform dielectric medium with a dielectric constant ε . If the electromagnetic field is uniform along the direction y ($\partial/\partial y \equiv 0$), then it can be decomposed into two separate waves of different polarizations. In the following we restrict our consideration to p -polarized waves, whose magnetic field is perpendicular to the plane of incidence (xz). Such a wave possesses the electromagnetic field components $\vec{E} = \{E_x, 0, E_z\}$, $\vec{H} = \{0, H_y, 0\}$, and is described by the Maxwell equations

$$\frac{\partial E_x}{\partial z} - \frac{\partial E_z}{\partial x} = i\kappa H_y, \quad (3)$$

$$\frac{\partial H_y}{\partial z} = i\kappa\varepsilon E_x, \quad \frac{\partial H_y}{\partial x} = -i\kappa\varepsilon E_z. \quad (4)$$

Here we assumed the temporal dependence of the electromagnetic field \vec{E}, \vec{H} in the form of $\exp(-i\omega t)$, where ω is the cyclic frequency, $\kappa = \omega/c$ and c is the speed of light in vacuum. The electromagnetic properties of the graphene layer are determined by its dynamical conductivity $\sigma_g(\omega)$, whose form can be found, e.g., in Ref.⁴¹. In order to find the dispersion relation of the graphene multilayer PC, the electromagnetic fields should be considered separately in each layer between the adjacent graphene sheets at planes $z = md$ and $z = (m+1)d$. The solutions of the Maxwell equations (3)–(4) at the spatial domain $md \leq z \leq (m+1)d$ can be represented as

$$H_y(x, z) = \{H_{m,+} \exp[ik_z(z - md)] + H_{m,-} \exp[-ik_z(z - md)]\} \exp(ik_x x), \quad (5)$$

$$E_x(x, z) = \frac{k_z}{\kappa\varepsilon} \{H_{m,+} \exp[ik_z(z - md)] - H_{m,-} \exp[-ik_z(z - md)]\} \exp(ik_x x) \quad (6)$$

$$E_z(x, z) = -\frac{k_x}{\kappa\varepsilon} \{H_{m,+} \exp[ik_z(z - md)] + H_{m,-} \exp[-ik_z(z - md)]\} \exp(ik_x x). \quad (7)$$

Here k_x is the in-plane component of the wavevector (parallel to the graphene sheets), $k_z = (\kappa^2\varepsilon - k_x^2)^{1/2}$, $H_{m,\pm}$ are the amplitudes of the forward (sign "+") or backward (sign "-") propagating waves. By matching boundary conditions at $z = md$ [continuity of the tangential component of the electric field across the graphene $E_x(x, md+0) = E_x(x, md-0)$, and discontinuity of the tangential component of the magnetic field, caused by

surface currents in graphene, $H_y(x, md+0) - H_y(x, md-0) = -(4\pi/c)j_x = -(4\pi/c)\sigma_g E_x(x, md)$, one can find that amplitudes $H_{m,\pm}$ can be related to $H_{m-1,\pm}$ as

$$\begin{pmatrix} H_{m,+} \\ H_{m,-} \end{pmatrix} = \hat{M} \begin{pmatrix} H_{m-1,+} \\ H_{m-1,-} \end{pmatrix}, \quad (8)$$

where the matrix \hat{M} reads as

$$\hat{M} = \begin{pmatrix} \exp(ik_z d) [1 - i\Lambda k_z] & i\Lambda k_z \exp(-ik_z d) \\ -i\Lambda k_z \exp(ik_z d) & \exp(-ik_z d) [1 + i\Lambda k_z] \end{pmatrix}$$

with $\Lambda = 2\pi\sigma_g/(i\omega\varepsilon)$. Since the considered structure is periodic, it is possible to use the Bloch theorem, which determines the proportionality between field amplitudes in the adjacent periods through the Bloch wavevector q :

$$H_{m-1,\pm} = \exp(-iqd) H_{m,\pm}, \quad (9)$$

After substitution of this relation into Eqs.(8), the solvability condition of the resulting linear equations requires (here \hat{I} is the unit matrix)

$$\text{Det} \left[\hat{M} - \exp(iqd) \hat{I} \right] = 0, \quad (10)$$

which results into the dispersion relation for the p -wave in graphene multilayer PC

$$\cos(qd) - \cos(k_z d) - \Lambda k_z \sin(k_z d) = 0. \quad (11)$$

Similar expressions for the dispersion relation were obtained in Ref.^{7,18}. The dispersion relation Eq.(11) for fixed ω and q possesses an infinite number of solutions for k_x . Further in the paper we will prescribe an index $n \geq 0$ as a superscript to all parameters distinguishing the respective eigenmode. We also note, that the solvability conditions for Eq.(10) [as well as the dispersion relation (11)] imply a simple relation between forward- and backward propagating waves

$$\begin{aligned} \frac{H_{m,+}^{(n)}}{H_{m,-}^{(n)}} &= -\frac{\exp(-ik_z^{(n)} d) \Lambda k_z^{(n)}}{\exp(ik_z^{(n)} d) [1 - \Lambda k_z^{(n)}] - \exp(iqd)} = \\ &= \frac{\exp(iqd) - \exp(-ik_z^{(n)} d)}{\exp(iqd) - \exp(ik_z^{(n)} d)}, \end{aligned}$$

which allows to represent these amplitudes as

$$H_{m,+}^{(n)} = \mathcal{H}^{(n)}(q, \omega) \frac{\exp(iqd) - \exp(-ik_z^{(n)} d)}{2\sqrt{A^{(n)}}} \exp(iqmd), \quad (12)$$

$$H_{m,-}^{(n)} = \mathcal{H}^{(n)}(q, \omega) \frac{\exp(iqd) - \exp(ik_z^{(n)} d)}{2\sqrt{A^{(n)}}} \exp(iqmd), \quad (13)$$

where $\mathcal{H}^{(n)}(q, \omega)$ is the magnetic field amplitude and $A^{(n)}$ is a normalization factor. Notice that amplitudes

being represented in this form also satisfy Bloch condition (9). Substituting Eqs.(12) and (13) into (5), we obtain the expression for the component of the electromagnetic field at spatial domain $md \leq z \leq (m+1)d$ in the form

$$H_{y,\pm}^{(n)}(x, z||q, \omega) = \mathcal{H}_{\pm}^{(n)}(q, \omega) \times \psi^{(n)}(z||q, \omega) \exp(\pm ik_x^{(n)} x), \quad (14)$$

$$E_{x,\pm}^{(n)}(x, z||q, \omega) = \frac{\mathcal{H}_{\pm}^{(n)}(q, \omega)}{i\kappa\varepsilon} \times \frac{\partial \psi^{(n)}(z||q, \omega)}{\partial z} \exp(\pm ik_x^{(n)} x), \quad (15)$$

$$E_{z,\pm}^{(n)}(x, z||q, \omega) = \mp \mathcal{H}_{\pm}^{(n)}(q, \omega) \frac{k_x^{(n)}}{\kappa\varepsilon} \times \psi^{(n)}(z||q, \omega) \exp(\pm ik_x^{(n)} x), \quad (16)$$

where

$$\begin{aligned} \psi^{(n)}(z||q, \omega) &= \left\{ \exp[iqd] \cos \left[k_z^{(n)}(z - md) \right] \right. \\ &\quad \left. - \cos \left[k_z^{(n)}(md + d - z) \right] \right\} \frac{\exp[iqmd]}{\sqrt{A^{(n)}}}, \end{aligned} \quad (17)$$

is a dimensionless spatial profile function. Here the normalization factor

$$\begin{aligned} A^{(n)} &= 1 - \cos(qd) \cos \left(k_z^{(n)} d \right) + \\ &\quad \frac{\cos \left(k_z^{(n)} d \right) - \cos(qd)}{k_z^{(n)} d} \sin \left(k_z^{(n)} d \right) \end{aligned}$$

is chosen to satisfy the condition

$$\frac{1}{d} \int_{md}^{md+d} \left| \psi^{(n)}(z||q, \omega) \right|^2 dz = 1.$$

Also we take into account that all eigenmodes of the PC can be either forward- or backward propagating: this fact is stressed in Eqs.(14)–(16) by adding the signs “+” or “-” before the x -component of wavevector $k_x^{(n)}$ as well as by the subscript in the amplitude $\mathcal{H}_{\pm}^{(n)}$.

Before considering the dispersion properties in detail, it should be noticed that further in the paper we neglect collisional losses and take the relaxation rate in graphene $\Gamma = 0$, i.e., the graphene conductivity is supposed to be purely imaginary. This approximation simplifies the analysis without changing quantitatively the results. The spatial periodicity of the multilayer graphene PC gives rise to the band-gap structure [see Fig.1(a)]: the spectrum is composed of an infinite number of bands [$n \geq 0$, colored domains in Fig.1(a)], whose boundaries are determined by the Bloch wavevector at the center $q = 0$, or at edge $q = \pi/d$ of Brillouin zone [bold solid and bold dashed lines in Fig.1(a), respectively]. One of the bands [$n = 0$, depicted by red color in Fig.1(a)] is polaritonic, where electromagnetic waves are evanescent in z -direction (with purely imaginary $k_z^{(0)}$), and propagating in x -direction (with purely

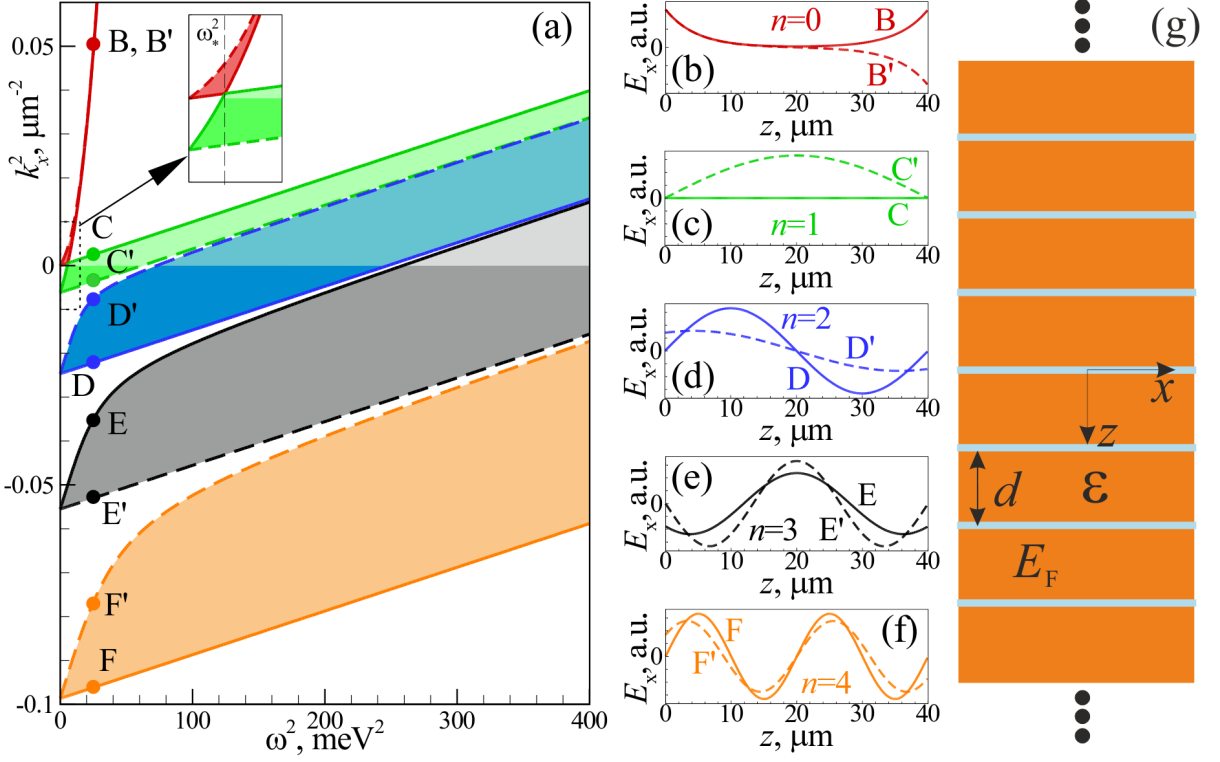


FIG. 1. (a) Dispersion curves (squared x -component of wavevector k_x^2 versus squared frequency ω^2) of graphene multilayer PC: colored domains correspond to the allowed bands, which boundaries are determined by Bloch wavevector at center of Brillouin zone $q = 0$ (bold solid lines, like B-F), or at its edge $q = \pi/d$ (bold dashed lines, like B'-F'); (b)-(f) Spatial profiles of the multilayer graphene PC's eigenfunctions at $\omega = 5$ meV. The parameters, which correspond to each of the eigenfunctions in panels (b)-(f), are depicted by respective points B-F, B'-F' in panel (a). In all panels other parameters are: $d = 40$ μm , $E_F = 0.157$ eV (which correspond to the gate voltage 25 V, applied to graphene on top of the 300 nm thickness SiO_2 substrate), $\epsilon = 3.9$, $\Gamma = 0$; (g) Schematic view of the graphene-based PC.

real $k_x^{(0)}$). The other bands ($n \geq 1$) are photonic ones, four of which with $n = 1, \dots, 4$ are depicted in Fig.1(a) by green, blue, black and orange colors, respectively. All photonic bands are characterized by the propagating nature of the electromagnetic waves in z -direction (with purely real $k_z^{(n)}$), while in x -direction they can be either propagating [$(k_x^{(n)})^2 > 0$, shaded by lighter colors in Fig.1(a)], or evanescent [$(k_x^{(n)})^2 < 0$, shaded by darker colors in Fig.1(a)]. The latter are physically meaningful only in confined photonic crystals because they diverge in either plus or minus infinity. Notice that, as follows from the inset in Fig.1(a), the polaritonic and the first photonic band touch each other at a cutoff frequency $\omega_* \approx (4\alpha E_F c / \hbar \epsilon d)^{1/2}$ in the center of the Brillouin zone, $q = 0$ (see Appendix A for details). Below this frequency, for $\omega < \omega_*$, the edge of the polaritonic band at $q = 0$ coincides with the light line $k_x^2 = \omega^2 \epsilon / c^2$, while above it, for $\omega > \omega_*$, the boundary of the polaritonic band $q = 0$ detaches from the light line [which coincides with the edge of the first photonic band, solid green line in Fig.1(a)]. At high frequencies, when the localization of the polaritonic modes near each graphene layer is strong,

and the SPPs, sustained by neighboring graphene layers, are almost noninteracting. This fact gives rise to the situation when polaritonic dispersion curves for different Bloch wavevectors q merge together [see e.g. points B and B' in Fig.1(a)], although their spatial profiles remain different, as it is evident from Fig.1(b).

Some of the edges of the photonic bands are characterized by an interesting property: at $q = \pi/d$ the edges of the photonic bands with odd numbers, $n = 2l - 1$ ($1 \leq l < \infty$) possesses z -components of the wavevector

$$k_z^{(2l-1)} = \left\{ \frac{\omega^2}{c^2} \epsilon - \left(k_x^{(2l-1)} \right)^2 \right\}^{1/2} = \frac{2l-1}{d} \pi. \quad (18)$$

Examples of such modes are C' and E' in Figs.1(c) and 1(e). Corresponding expressions for the eigenfunctions (17) can be represented as (details can be found in Appendix A)

$$\psi^{(2l-1)} \left(z \parallel \frac{\pi}{d}, \omega \right) = \sqrt{2} \cos \left[\frac{2l-1}{d} \pi z \right]. \quad (19)$$

When $q = 0$, the edges of the bands with even numbers

$n = 2l$ ($1 \leq l < \infty$) possess the same property, i.e.

$$k_z^{(2l)} = \left\{ \frac{\omega^2}{c^2} \varepsilon - \left(k_x^{(2l)} \right)^2 \right\}^{1/2} = \frac{2l}{d} \pi, \quad (20)$$

$$\psi^{(2l)}(z||0, \omega) = \sqrt{2} \cos \left[\frac{2l}{d} \pi z \right]. \quad (21)$$

Examples of such modes are D and F in Figs.1(d) and 1(f). It is interesting that expressions for solutions (18), (20) do not contain the graphene conductivity σ_g (in other words, their spectrum does not depend upon the graphene's Fermi energy E_F): z -components $k_z^{(2l)}$ and $k_z^{(2l-1)}$, specified by Eqs.(18) and (20), cancel conductivity-dependent term in the dispersion relation (11). This happens because the derivatives of their spatial profile functions vanish, $\partial\psi^{(n)}/\partial z=0$ at $z = md$ [see (19), (21)]. According to (15), it implies zero tangential components of the electric field $E_{x,\pm}^{(n)}(x, md||q) = 0$ at graphene layers, clearly seen from the spatial profiles of the modes C', D, E', F in Figs.1(c)–1(f). The light line $k_x = \omega\sqrt{\varepsilon}/c$ mentioned above is also an eigenmode of the multilayer graphene PC with $q = 0$ [see mode C in Fig.1(c)]. It is characterized by absence of the wavevector's z -component $k_z^{(n)} = 0$ and the spatial profile function $\psi^{(n)}(z||0, \omega) = 1$ (further in the paper this mode will be referred to as the *light-line mode*). The band index for this mode is $n = 0$ in the frequency domain $\omega < \omega_*$ (where this mode is the edge of polaritonic band) and $n = 1$ above the critical frequency $\omega > \omega_*$ (where this mode is the edge of the first photonic band). As a matter of fact, this mode is a bulk electromagnetic wave propagating in the x -direction and with zero longitudinal component of the electric field $E_x^{(n)}(x, z||q, \omega) \equiv 0$, i.e. a purely transverse wave.

III. SCATTERING OF POLARITONIC MODE FROM A SINGLE INTERFACE BETWEEN TWO GRAPHENE MULTILAYER PCS

Let us consider now an interface between two graphene multilayer PCs (described in Sec.II). We suppose that both PCs possess the same period d , are embedded in the same homogeneous dielectric medium with the dielectric permittivity ε , and graphene layers are arranged in the same planes $z = md$ along axis z . The only difference between these graphene multilayer PCs is the Fermi energy, which is equal to E_{F1} in the first PC (occupying the half-space $x < 0$) and to E_{F2} in the second one (occupying the half-space $x > 0$). Further in the text the left and right PCs will be referred to as PC1 and PC2, respectively. Such an interface is schematically depicted in Fig.2. We consider the situation, where the polaritonic mode propagates in the positive direction of the x -axis (thus coming from $x = -\infty$) and impinges on the aforementioned interface. The main objective of the present section is to describe the scattering of the polaritonic mode on this interface, that is, we want to find the

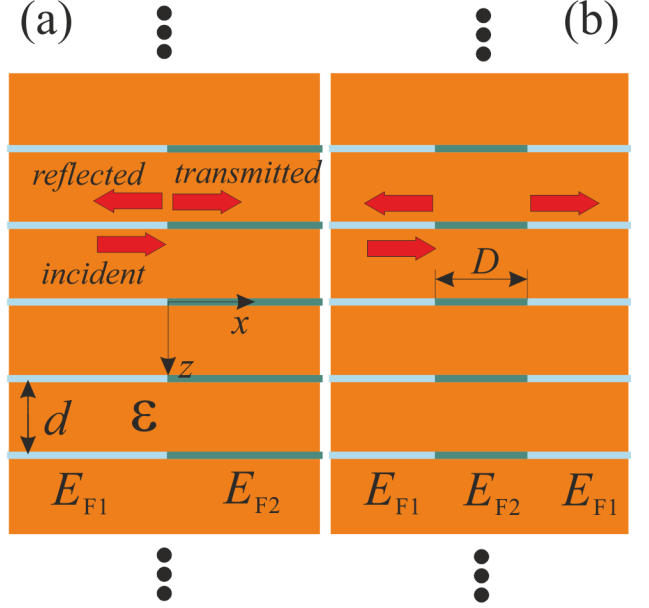


FIG. 2. A single [panel (a)] or double [panel (b)] interface between two graphene multilayer PCs with different Fermi energies of graphene layers.

transmission and reflection coefficients of the polaritonic mode as well as to determine which part of its energy is transferred to each of the photonic modes.

In order to do this, we expand the electromagnetic field in series with respect to the graphene multilayer PC eigenmodes (14)–(16). So, the magnetic field and the z -component of the electric field in PC1 ($x < 0$) can be written as

$$H_{1,y}(x, z) = \mathcal{H}_{1,+}^{(0)} \psi_1^{(0)}(z) \exp(ik_{1,x}^{(0)}x) + \sum_{n=0}^{\infty} \mathcal{H}_{1,-}^{(n)} \psi_1^{(n)}(z) \exp(-ik_{1,x}^{(n)}x), \quad (22)$$

$$E_{1,z}(x, z) = -\mathcal{H}_{1,+}^{(0)} \frac{k_{1,x}^{(0)}}{\kappa\varepsilon} \psi_1^{(0)}(z) \exp(ik_{1,x}^{(0)}x) + \sum_{n=0}^{\infty} \mathcal{H}_{1,-}^{(n)} \frac{k_{1,x}^{(n)}}{\kappa\varepsilon} \psi_1^{(n)}(z) \exp(-ik_{1,x}^{(n)}x). \quad (23)$$

In the same manner, the fields in PC2 can be expressed as

$$H_{2,y}(x, z) = \sum_{l=0}^{\infty} \mathcal{H}_{2,+}^{(l)} \psi_2^{(l)}(z) \exp(ik_{2,x}^{(l)}x), \quad (24)$$

$$E_{2,z}(x, z) = -\sum_{l=0}^{\infty} \mathcal{H}_{2,+}^{(l)} \frac{k_{2,x}^{(l)}}{\kappa\varepsilon} \psi_2^{(l)}(z) \exp(ik_{2,x}^{(l)}x). \quad (25)$$

In Eqs.(22)–(25) we prescribe the PC index $j = 1, 2$ to the spatial profile function $\psi_j^{(n)}$, the x -component of wavevector $k_{j,x}^{(n)}$, and the amplitude $\mathcal{H}_{j,\pm}^{(n)}$. Also we use

band indices n and l , referring to PC1 and PC2, respectively, and drop the arguments q and ω (which are equal for PC1 and PC2) in functions and amplitudes for brevity. Notice that Eqs.(22) and (23) contain only one mode (polaritonic one with index $n = 0$) propagating towards the interface in PC1 (referring to the above-mentioned incident wave with amplitude $\mathcal{H}_{1,+}^{(0)}$) and a full set of modes propagating backward from the interface (corresponding to the reflected harmonics with amplitudes $\mathcal{H}_{1,-}^{(n)}$). At the same time, Eqs.(24) and (25) contain only modes propagating in PC2 in the positive direction of x -axis, which correspond to the transmitted modes with amplitudes $\mathcal{H}_{2,+}^{(m)}$.

The next step is to apply the boundary conditions at the interface $x = 0$ [continuity of tangential components of magnetic field $H_{1,y}(0, z) = H_{2,y}(0, z)$, and electric field $E_{1,z}(0, z) = E_{2,z}(0, z)$] and use the orthogonality of the spatial profile functions,

$$\int_{md}^{md+d} \psi_j^{(n')} (z) \overline{\psi_j^{(n)}} (z) dz = \delta_{n,n'} d,$$

where the overbar denotes complex conjugation. After applying this orthogonality conditions to Eqs.(22)–(25) we obtain the following equations for the amplitudes:

$$\delta_{n,0} \mathcal{H}_{1,+}^{(0)} + \mathcal{H}_{1,-}^{(n)} = \sum_{l=0}^{\infty} \mathcal{H}_{2,+}^{(l)} \Psi_{l,n}, \quad (26)$$

$$\left[\delta_{n,0} \mathcal{H}_{1,+}^{(0)} - \mathcal{H}_{1,-}^{(n)} \right] k_{1,x}^{(n)} = \sum_{l=0}^{\infty} k_{2,x}^{(l)} \mathcal{H}_{2,+}^{(l)} \Psi_{l,n}, \quad (27)$$

where

$$\Psi_{l,n} = \frac{1}{d} \int_{md}^{md+d} \psi_2^{(l)} (z) \overline{\psi_1^{(n)}} (z) dz. \quad (28)$$

It should be noticed that the obtained Eqs.(26) and (27) can also be applied to the case of an interface between the PC and a homogeneous medium (formally in this case $E_{F2} = 0$). In this case the spatial profile functions will be as follows:

$$\psi_2^{(l)} (z) = \exp \left(i k_z^{(l)} z \right), \quad (29)$$

$$k_z^{(l)} = q + \frac{2l}{d} \pi = \sqrt{\kappa^2 \varepsilon - \left(k_x^{(l)} \right)^2}. \quad (30)$$

In order to express the reflection and transmission coefficients in terms of energy fluxes, we notice that the component of the Poynting vector along the direction of propagation (x -axis) for the n -th mode $S_{j,\pm}^{(n)} = -(c/8\pi) \operatorname{Re} \left(E_{j,z,\pm}^{(n)} \overline{H_{j,y,\pm}^{(n)}} \right)$, after substituting the explicit forms of the electromagnetic fields (22)–(25), can be written as

$$S_{j,\pm}^{(n)} = \pm \frac{c}{8\pi \kappa \varepsilon} \operatorname{Re} \left(k_{j,x}^{(n)} \left| \mathcal{H}_{j,\pm}^{(n)} \right|^2 \left| \psi_j^{(n)} (z) \right|^2 \right).$$

In other words, if the mode is propagating (with purely real $k_x^{(n)}$), it carries energy either in positive (sign “+”)

or in negative (sign “-”) direction of x -axis. In contrast, evanescent modes (with purely imaginary $k_x^{(n)}$) do not carry any energy. Thus, we define the coefficients R_n, T_l as the integral characteristics

$$R_n = - \frac{\int_{md}^{md+d} S_{1,-}^{(n)} dz}{\int_{md}^{md+d} S_{1,+}^{(0)} dz} = \frac{\operatorname{Re} \left(k_{1,x}^{(n)} \right) \left| \mathcal{H}_{1,-}^{(n)} \right|^2}{\operatorname{Re} \left(k_{1,x}^{(0)} \right) \left| \mathcal{H}_{1,+}^{(0)} \right|^2}, \quad (31)$$

$$T_l = \frac{\int_{md}^{md+d} S_{2,+}^{(l)} dz}{\int_{md}^{md+d} S_{1,+}^{(0)} dz} = \frac{\operatorname{Re} \left(k_{2,x}^{(l)} \right) \left| \mathcal{H}_{2,+}^{(l)} \right|^2}{\operatorname{Re} \left(k_{1,x}^{(0)} \right) \left| \mathcal{H}_{1,+}^{(0)} \right|^2}. \quad (32)$$

The coefficients R_0, T_0 are the reflectance and the transmittance of the polaritonic mode, respectively, while the others ($n \neq 0$) are normalized intensities of higher diffraction orders in PC1 and PC2 (coefficients R_n and T_l , respectively).

First, we will consider the scattering of an incident polaritonic mode on the interface between the graphene multilayer PC and a homogeneous dielectric, schematically depicted in Fig.3(i). As it was mentioned, in the case $q = 0$ [left column in Fig.3] the polaritonic mode exists in the frequency range $\omega > \omega_{*1} \approx 2.4$ meV only [light gray, white and yellow domains in Figs.3(a)–3(d)], while the existence of polaritonic mode below the cutoff frequency, $\omega < \omega_{*1}$ is impossible [dark gray domains in in Figs.3(a)–3(d)]. In the frequency range $\omega_{*1} < \omega < 2\pi c/\sqrt{\varepsilon} d \approx 15.8$ meV [light gray domain in Figs.3(a)–3(d)] there are only two propagating modes in the PC1, namely, polaritonic mode with $n = 0$ [depicted by red line in Fig.3(a)] and the light-line mode $n = 1$ [depicted by green line in Fig.3(a)]. In the homogeneous dielectric in this frequency range there is only one propagating mode with $l = 0$ [see Eq.(29)]. Notice the coincidence of both the shape and dispersion properties of modes with $l = 0$ in the homogeneous dielectric and the light-line mode in PC1. Nevertheless, due to the opposite parity⁴² of the spatial profile functions integral (28) $\Psi_{0,0}(0) \equiv 0$, i.e. polaritonic mode can not be coupled to the light-line mode, thus giving rise to the total reflection ($R_0 = 1$) of the polaritonic mode in this frequency range, shown in Fig.3(b).

The narrow frequency range $15.8 \text{ meV} \lesssim \omega \lesssim 16.1 \text{ meV}$ [white domain in Figs.3(a)–3(d)] corresponds to the situation when one more mode in PC with $n = 2$ [depicted by blue line in Fig.3(a)] as well as two more modes in the homogeneous dielectric, with $l = -1, 1$ become propagating. In spite of having the same dispersion properties [compare Eqs.(20) and (30)], these modes possess different spatial profiles [compare Eqs.(21) and (29)]. The incident polaritonic mode $n = 0$, although not being able to couple to the mode $n = 2$ in PC due to the opposite parity [see modes B in Fig.1(b) and D in Fig.1(d)], still can couple to the modes $l = -1, 1$ in the homogeneous dielectric. The last fact results in the nonzero intensities of these diffraction orders T_{-1} and T_1 , shown in Fig.3(d), and a decrease of the polaritonic mode re-

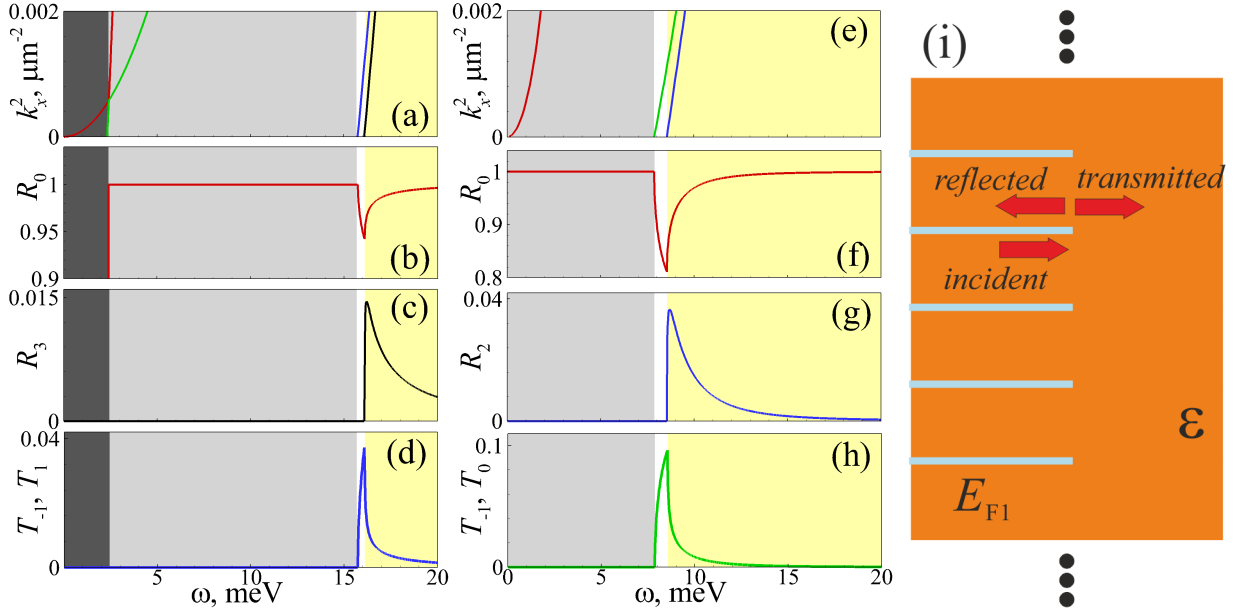


FIG. 3. (a,e) Dispersion curves [the same as in Fig.1(a)] of graphene multilayer PC for $q = 0$ [panel (a)], or for $q = \pi/d$ [panel (e)]; (b)–(d), (f)–(h) Frequency dependence of the reflectance $R_n(\omega)$ of polaritonic mode $n = 0$ [panels (b) and (f)], diffraction order intensities of PC modes $n = 3$ or $n = 2$ [correspondingly panels (c) and (g)] and those $T_l(\omega)$ of homogeneous dielectric modes $l = -1$ and $l = -1$ [panel (d)] or $l = -1$ and $l = 0$ [panel (h)] for the case when the polaritonic mode with Bloch wavevector $q = 0$ [left column, panels (b)–(d)] or $q = \pi/d$ [central column, panels (f)–(h)] is scattered from the interface between the graphene multilayer PC and homogeneous medium. The parameters of the structure under consideration are $\varepsilon = 3.9$, $E_{F1} = 0.157$ eV, $d = 40$ μm . Notice that in panel (d) transmission coefficients for modes $l = -1$ and $l = 1$ are equal to each other [as well as in panel (h) transmission coefficients for modes for $l = -1$ and $l = 0$ are also equal]; (i) Schematic view of the interface between the graphene-based PC and a homogeneous medium.

flectance [Fig.3(b)]. At higher frequencies, $\omega \gtrsim 16.1$ meV [yellow domain in Figs.3(a)–3(d)] there is one more propagating mode with $n = 3$ in the PC1 with the same parity as the incident polaritonic mode [compare modes B in Fig.1(b) and E in Fig.1(e)], thus allowing their coupling and nonzero intensity of diffraction order R_3 [Fig.3(c)]. Nevertheless, the third diffraction order intensity R_3 is a decreasing function of frequency. At the same time, the diffraction intensities T_{-1} , T_1 and the reflectance R_0 [see Figs.3(d) and 3(b)] possess a maximum and a minimum, correspondingly, at the boundary of the white and the yellow domains, $\omega \approx 16.1$ meV.

The diffraction of the polaritonic mode with $q = \pi/d$ [central column in Fig.3] is characterized by the following interesting features. In this case the polaritonic mode $n = 0$ can exist at any frequency [red line in Figs.3(e)], thus total reflectance ($R_0 \equiv 1$) takes place [Fig.3(f)] in the frequency range $\omega \lesssim 7.9$ meV. This frequency range is depicted by light gray shadow in Figs.3(e)–3(h). In the frequency range 7.9 meV $\lesssim \omega \lesssim 8.5$ meV [white domain in Figs.3(e)–3(h)] the energy of the incident mode is partially transformed into that of the propagating modes $l = -1, 0$ of the homogeneous dielectric [green line in Fig.3(e)], giving rise to nonzero diffraction orders intensities T_{-1} and T_0 [Fig.3(h)]. At the same time, in the frequency range $\omega \gtrsim 8.5$ meV [yellow domain in Figs.3(e)–3(h)] the coupling between the polaritonic mode and the

photonic mode with $n = 2$ becomes possible [Fig.3(g)].

The characteristics of the diffraction of the polaritonic mode at the interface between two graphene multilayer PCs are shown in Fig.4. As in the previous case, polaritonic modes for $q = 0$ exist above the cutoff frequencies ω_{*1} and ω_{*2} in the PC1 and PC2, respectively [nonexistence domain $\omega < \omega_{*1}$ is depicted in Figs.4(a) and 4(b) by dark gray color]. The frequency range $\omega_{*1} < \omega \lesssim 3.1$ meV [light gray domain in Figs.4(a) and 4(b)] is characterized by the existence of polaritonic mode in the PC1, while in the PC2 there is only one propagating mode (the light-line one). Owing to the above-mentioned opposite parity of these modes, mutual coupling between them is not possible, which results in the total reflection $R_0 = 1$ [see Fig.4(b)] of the polaritonic mode from the interface between two PCs. In the frequency range $\omega \gtrsim 3.1$ meV [white domain in Figs.4(a) and 4(b)] the PC2 contains one more propagating mode, which is photonic ($n = 1$) below the cutoff frequency ω_{*2} and polaritonic ($n = 0$) above it. The last fact gives rise to a gradual decrease of the reflectance and an increase of the transmittance [Fig.4(b)] of the incident polaritonic mode. At the same time, when $q = \pi/d$ there is no cut-off frequency for the existence of polaritonic mode [see Fig.4(c)], which results in the nonzero transmittance at any frequency [Fig.4(d)]. It is interesting that for $q = \pi/d$ (contrary to the case of $q = 0$) the reflectance (transmit-

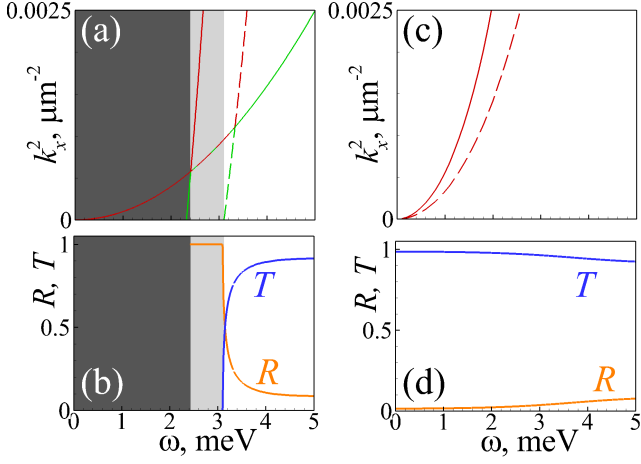


FIG. 4. (a), (c) Dispersion curves of graphene multilayer PC with E_{F1} (solid lines) or E_{F2} (dashed lines) for $q = 0$ [panel (a)], or for $q = \pi/d$ [panel (c)]; (b), (d) Frequency dependence of the reflectance $R_0(\omega)$ and the transmittance $T_0(\omega)$ of polaritonic mode with Bloch wavevector $q = 0$ [panel (b)] or $q = \pi/d$ [panel (d)] when it is diffracted on the interface between two graphene multilayer PCs with Fermi energies E_{F1} and E_{F2} . The parameters of the structure under consideration are: $\varepsilon = 3.9$, $E_{F1} = 0.157$ eV, $E_{F2} = 0.3$ eV, $d = 40$ μm .

tance) is an increasing (decreasing) function of frequency [compare Figs.4(b) and 4(d)].

IV. SCATTERING OF POLARITONIC MODE FROM THE DOUBLE INTERFACE BETWEEN TWO GRAPHENE MULTILAYER PCS

We now consider the situation [Fig.2(b)] when a graphene multilayer PC of finite width D (along the x -axis) and with graphene layer's Fermi energy E_{F2} (further referred to as PC2) is cladded by two semi-infinite PCs which graphene layer are characterized by the Fermi energy E_{F1} (these two PCs will be referred to as PC1 and PC3). As in Sec.II, the incident wave is the polaritonic mode of PC1, propagating in the positive direction of the x -axis. Notice, that the only difference between Fig.2(a) and 2(b) is the presence of two interfaces in the last case.

We note that the electromagnetic field in the region $x < 0$ can be represented in the same manner as in Eqs.(22) and (23), while inside the region $0 < x < D$, occupied by the PC2, the field components will have the form:

$$H_{2,y}(x, z) = \sum_l \psi_2^{(l)}(z) \times [\mathcal{H}_{2,+}^{(l)} \exp(ik_{2,x}^{(l)}x) + \mathcal{H}_{2,-}^{(l)} \exp(-ik_{2,x}^{(l)}x)], \quad (33)$$

$$E_{2,z}(x, z) = - \sum_l \frac{k_{2,x}^{(l)}}{\kappa\varepsilon} \psi_2^{(l)}(z) \times [\mathcal{H}_{2,+}^{(l)} \exp(ik_{2,x}^{(l)}x) - \mathcal{H}_{2,-}^{(l)} \exp(-ik_{2,x}^{(l)}x)]. \quad (34)$$

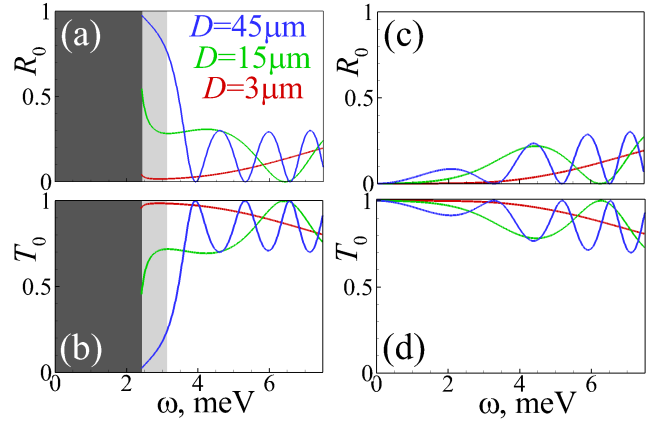


FIG. 5. Reflectance [panels (a) and (c)] and transmittance [panels (b) and (d)] versus frequency ω for the double interface between two graphene multilayer PCs with parameters $\varepsilon = 3.9$, $E_{F1} = 0.157$ eV, $E_{F2} = 0.3$ eV, $d = 40$ μm , $q = 0$ [panels (a) and (b)], or $q = \pi/d$ [panels (c) and (d)], $D = 45$ μm (blue lines), $D = 15$ μm (green lines), $D = 3$ μm (red lines).

Due to the finite width D of the PC2, Eqs.(33) and (34) contain both forward- and backward propagating waves. Finally, in the PC3 (region $x > D$) the electromagnetic field components are:

$$H_{3,y}(x, z) = \sum_n \mathcal{H}_{3,+}^{(n)} \psi_1^{(n)}(z) \times \exp[ik_{1,x}^{(n)}(x - D)], \quad (35)$$

$$E_{3,z}(x, z) = - \sum_n \mathcal{H}_{3,+}^{(n)} \frac{k_{1,x}^{(n)}}{\kappa\varepsilon} \psi_1^{(n)}(z) \times \exp[ik_{1,x}^{(n)}(x - D)]. \quad (36)$$

Applying the same boundary condition as in Sec.III, we have:

$$\delta_{n,0} \mathcal{H}_{1,+}^{(0)} + \mathcal{H}_{1,-}^{(n)} = \sum_l \Psi_{l,n} [\mathcal{H}_{2,+}^{(l)} + \mathcal{H}_{2,-}^{(l)}], \quad (37)$$

$$[\delta_{n,0} \mathcal{H}_{1,+}^{(0)} - \mathcal{H}_{1,-}^{(n)}] k_{1,x}^{(n)} = \quad (38)$$

$$\sum_l k_{2,x}^{(l)} \Psi_{l,n} [\mathcal{H}_{2,+}^{(l)} - \mathcal{H}_{2,-}^{(l)}],$$

$$\mathcal{H}_{3,+}^{(n)} = \sum_l \Psi_{l,n} \times \quad (39)$$

$$[\mathcal{H}_{2,+}^{(l)} \exp(ik_{2,x}^{(l)}D) + \mathcal{H}_{2,-}^{(l)} \exp(-ik_{2,x}^{(l)}D)],$$

$$\mathcal{H}_{3,+}^{(n)} k_{1,x}^{(n)} = \sum_l k_{2,x}^{(l)} \Psi_{l,n} \times \quad (40)$$

$$[\mathcal{H}_{2,+}^{(l)} \exp(ik_{2,x}^{(l)}D) - \mathcal{H}_{2,-}^{(l)} \exp(-ik_{2,x}^{(l)}D)].$$

For this structure the coefficients T_n are expressed as

$$T_n = \frac{\int_{md}^{md+d} S_{2,+}^{(n)} dz}{\int_{md}^{md+d} S_{1,+}^{(0)} dz} = \frac{\text{Re}(k_{1,x}^{(n)}) |\mathcal{H}_{3,+}^{(n)}(q)|^2}{\text{Re}(k_{1,x}^{(0)}) |\mathcal{H}_{1,+}^{(0)}(q)|^2},$$

while the coefficients R_n are the same as before [Eq.(31)].

The frequency dependence of the reflectance and transmittance for this structure are shown in Fig.5. For $q = 0$ and large width of the PC2 [light gray domain in Figs.5(a) and 5(b)] the reflectance [blue line in Fig.5(a)] of the structure is slightly less than unity in the frequency range $\omega_{*1} < \omega \lesssim 3.1$ meV and it is a decreasing function of the frequency, while the transmittance is nonzero and is an increasing function of ω (compare with Fig.4(b), where in the case of single interface this range corresponds to the total reflectance $R_0 = 1$, $T_0 = 0$). The reason for this is the tunneling through the region $0 < x < D$ because there is no propagating mode in PC2. The tunneling rate (and, as a consequence, the transmittance T_0) gradually grows when the PC2 width, D is decreased, compare blue, green and red lines in Fig.5(b). Notice that for small $D = 3 \mu\text{m}$ [red line in Fig.5(b)] almost the whole energy of the incident wave is transmitted via tunneling, thus giving $T_0 \gtrsim 1$. In the frequency range $\omega \gtrsim 3.1$ meV [white domain in Figs.5(a) and 5(b)] one more mode in PC2 becomes propagating, which gives rise to the Fabry-Pérot oscillations of the transmittance and reflectance and the possibility of total transmission $T_0 = 1$ (respectively, $R_0 = 0$). The latter takes place at frequencies, for which the width D matches an integer number of polaritonic mode half-wavelengths, that is

$$k_{2,x}^{(0)} D = l\pi, \quad l \geq 1. \quad (41)$$

The same phenomenon also occurs when $q = \pi/d$ [see Figs.5(c) and 5(d)]. The frequencies at which full transmission takes place can be approximated using the Drude model for graphene's conductivity. Correspondingly, the parameter Λ in the dispersion relation (11) can be approximated by $\Lambda = 2\alpha c E_{F2} / \hbar \omega^2 \varepsilon$, while we also use the so-called non-retarded approximation for $k_{2,x}^{(0)} = -ik_z^{(0)}$. Under these assumptions the dispersion relation (11) can be rewritten as

$$\cos(qd) - \cosh\left(k_{2,x}^{(0)} d\right) + \Lambda k_{2,x}^{(0)} \sinh\left(k_{2,x}^{(0)} d\right) = 0,$$

which along with Eq.(41) gives

$$\omega^2 = \frac{2\alpha c E_{F2}}{\hbar \varepsilon} \frac{l\pi}{D} \frac{\sinh\left(\frac{l\pi}{D} d\right)}{\cosh\left(\frac{l\pi}{D} d\right) - \cos(qd)}. \quad (42)$$

For the case $D = 15 \mu\text{m}$ Eq.(42) gives $\omega \approx 6.82$ meV for $q = 0$ and $\omega \approx 6.81$ meV for $q = \pi/d$, which qualitatively agrees with Figs.5(b) and 5(d) [green line].

The oscillations of the transmittance can be seen as an optical analogue of the well known effect of electron resonant tunneling in a double-barrier heterostructure (DBHS).⁴³ The modulation depth of the electromagnetic wave transmission is smaller than in the case of electrons because of the weaker confinement of the former (so that direct tunneling involving only evanescent waves in the PC2 is possible) and also because of the simultaneous presence of several scattering channels.

V. CONCLUSIONS

We have analysed the scattering of surface plasmon-polaritons generated in a graphene multilayer photonic crystal and propagating across its lateral surface or interface with another graphene multilayer PC with a different band structure (controlled by the graphene's Fermi energy). In particular, for the low-frequency region where only the polaritonic mode (with imaginary z component of the wavevector, k_z) is propagating in the direction along the graphene sheets (while the modes with real k_z have imaginary k_x , i.e. are evanescent in this sense), we have shown that this mode is totally reflected from the interface between the graphene multilayer PC and a homogeneous dielectric. Nevertheless, in the higher-frequency region where photonic (i.e. propagating with real k_z) modes are allowed, the partial transformation of the incident polaritonic mode's energy into that of other diffraction orders (both in PC and in homogeneous dielectric) becomes possible, thus reducing the reflectance of the incident wave. Moreover, by virtue of the reciprocity principle this gives rise to the possibility to excite the PC's polaritonic eigenmode by an external wave impinging on its edge. In-phase polaritonic mode (with $q = 0$) can also be totally reflected from the interface between two PCs, while for out-of-phase oscillations (with $q \neq 0$) this scenario is impossible. It is also shown that the transmittance and the reflectance of a structure consisting of three photonic crystals and two interfaces between them (we asumed PC1=PC3≠PC2) exhibit Fabry-Pérot oscillations with a discrete set of frequencies for which total transmission of the polaritonic mode takes place. This effect is similar to the resonant tunneling of electrons in a DBHS where the electric current shows a sharp peak as a function of bias.⁴³ Here, in addition to the difference between the Fermi levels of the crystals PC1 and PC2, the electromagnetic wave transmission depends also on the PC wavevector q .

ACKNOWLEDGMENTS

We acknowledge support from the EC under the Graphene Flagship (Contract No. CNECT-ICT-649953).

Appendix A: Approximations for the eigenvalues and eigenfunctions.

Let us consider first the asymptotical behaviour of the polaritonic modes $n = 0$ at high frequencies, where the modes with different Bloch wavevector q merge. Since SPPs are evanescent waves, it is natural to introduce a decay parameter in z -direction, $p = -ik_z^{(0)}$. In this case the dispersion relation (11) can be rewritten as

$$p = \frac{\cosh(pd) - \cos(qd)}{\Lambda \sinh(pd)}. \quad (A1)$$

Notice that in the limiting case $d \rightarrow \infty$ the dispersion relation (A1) transforms into $p = \Lambda^{-1}$, i.e. into the dispersion relation for a single graphene sheet. If we consider the situation of d being large but finite, the single sheet dispersion relation can be used as zeroth approximation for p . This approximation after being substituted into the right hand side of Eq.(A1), allows for an approximate representation of Eq.(A1) as

$$p = \sqrt{\left(k_x^{(0)}\right)^2 - \kappa^2 \varepsilon} = \frac{1 - \cos(qd) \exp(-d/\Lambda)}{\Lambda}. \quad (\text{A2})$$

The above-mentioned zeroth approximation for p also can be used for approximating the spatial profile function (17), namely:

$$\begin{aligned} \psi^{(0)}(z||q, \omega) &= \left\{ \exp[iqd] \cosh[\Lambda^{-1}(z - md)] - \right. \\ &\quad \left. \cosh[\Lambda^{-1}(md + d - z)] \right\} \frac{\exp[iqmd]}{\sqrt{A^{(0)}}}, \\ A^{(0)} &= 1 - \cos(qd) \cosh(\Lambda^{-1}d) + \\ &\quad \Lambda \frac{\cosh(\Lambda^{-1}d) - \cos(qd)}{d} \sinh(\Lambda^{-1}d). \end{aligned}$$

Even more, since all the phenomena we are interested in take place in the frequency range $\hbar\omega \ll E_F$, we can take into account only the Drude contribution to graphene's conductivity. Correspondingly, the parameter Λ can be approximated by $\Lambda = 2\alpha c E_F / \hbar\omega^2 \varepsilon$.

This fact can be used in the approximation of the touching point (cutoff frequency) between the zeroth and first band at $q = 0$, mentioned in Sec.II. Taking into account the smallness of k_z in the touch points, one can expand the dispersion relation (11) as

$$\cos(qd) - 1 + \frac{(k_z d)^2}{2} - \frac{(k_z d)^4}{24} - \Lambda k_z \left[k_z d - \frac{(k_z d)^3}{6} \right] = 0.$$

At $q = 0$ we have

$$k_z^2 = \frac{12d - 2\Lambda}{d^2 d - 4\Lambda}.$$

Taking into account the above-mentioned approximation for Λ we find that $k_z^2 > 0$ (with $k_z^{(0)}$ being purely real) or $k_z^2 < 0$ (with $k_z^{(1)}$ being purely imaginary) in the frequency ranges $\omega < \omega_* = (4\alpha E_F c / \hbar d \varepsilon)^{1/2}$ and $\omega > \omega_*$, respectively. The last fact well corroborates with the dispersion curve behavior in the vicinity of the cutoff frequency ω_* , depicted in Fig.1(a).

From Fig.1(a) it is evident that in the high-frequency region $\omega \gg \omega_*$ the gaps becomes narrow. We can use this fact in order to approximate the eigenfunctions and the eigenvalues in this region. At the edge of the Brillouin zone ($q = \pi/d$) we represent z -component of the wavevector in the band with even number $n = 2l$ ($1 \leq l < \infty$) as $k_z^{(2l)} = k_z^{(2l-1)} + \Delta^{(2l)}$ with $\Delta^{(2l)}$ being small value ($|\Delta^{(2l)}| \ll |k_z^{(2l-1)}|$) and $k_z^{(2l-1)}$ is determined in Eq.(18). In this case the dispersion relation after the expansion of sine and cosine with respect to $\Delta^{(2l)}$ can be represented as

$$-\frac{(\Delta^{(2l)}d)^2}{2} + \Lambda \left[\frac{2l-1}{d} \pi + \Delta^{(2l)} \right] \Delta^{(2l)} d = 0,$$

from which it is possible to determine

$$\Delta^{(2l)} = \frac{2l-1}{d} \pi \frac{2\Lambda}{d-2\Lambda}$$

and

$$k_z^{(2l)} = \pi \frac{2l-1}{d-2\Lambda}.$$

In the same manner it is possible to obtain an approximate expression for the spatial profile function (17):

$$\begin{aligned} \psi^{(2l)}\left(z||\frac{\pi}{d}, \omega\right) &= (-1)^m \left\{ \sin\left[\frac{2l-1}{d}\pi z\right] - \right. \\ &\quad \frac{\Delta^{(2l)}}{2} \cos\left[\frac{2l-1}{d}\pi z\right] [(2m+1)d - 2z] - \\ &\quad \frac{(\Delta^{(2l)})^2}{6} \sin\left[\frac{2l-1}{d}\pi z\right] \times \\ &\quad \left. [d^2 - 3(z-md)(z-md-d)] \right\} \sqrt{\frac{2}{A^{(2l)}}}, \end{aligned} \quad (\text{A3})$$

with

$$\begin{aligned} A^{(2l)} &= 1 - \frac{\Delta^{(2l)}d}{(2l-1)\pi} - \\ &\quad \left(\frac{1}{12} - \frac{1}{(2l-1)^2 \pi^2} \right) (\Delta^{(2l)}d)^2. \end{aligned}$$

The same formalism can be applied to the boundaries of the bands with an odd numbers $n = 2l + 1$ ($1 \leq l < \infty$) at the center of Brillouin zone $q = 0$. Thus, we obtain

$$\Delta^{(2l+1)} = \frac{2l}{d} \pi \frac{2\Lambda}{d-2\Lambda}$$

and

$$k_z^{(2l+1)} = k_z^{(2l)} + \Delta^{(2l+1)} = \pi \frac{2l}{d-2\Lambda}.$$

An approximate expression for the spatial profile function (17) can be written

$$\begin{aligned} \psi^{(2l+1)}(z||0) &= \left\{ \sin\left[\frac{2l}{d}\pi z\right] - \right. \\ &\quad \frac{\Delta^{(2l+1)}}{2} \cos\left[\frac{2l}{d}\pi z\right] [(2m+1)d - 2z] - \\ &\quad \frac{(\Delta^{(2l+1)})^2}{6} \sin\left[\frac{2l}{d}\pi z\right] \times \\ &\quad \left. [d^2 - 3(z-md)(z-md-d)] \right\} \sqrt{\frac{2}{A^{(2l+1)}}}, \end{aligned} \quad (\text{A4})$$

with

$$A^{(2l+1)} = 1 - \frac{\Delta^{(2l+1)}d}{2l\pi} - \left(\frac{1}{12} - \frac{1}{4l^2\pi^2} \right) (\Delta^{(2l+1)}d)^2.$$

- ¹ S. A. Maier, *Plasmonics: Fundamentals and Applications* (Springer, New York, 2007).
- ² T. Low and P. Avouris, *ACS Nano* **8**, 1086 (2014).
- ³ J. A. Dionne and H. A. Atwater, *MRS Bulletin* **37**, 717 (2012).
- ⁴ M. I. Stockman, *Phys. Today* **64**, 39 (2011).
- ⁵ J. B. Khurgin and A. Boltasseva, *MRS Bulletin* **37**, 768 (2012).
- ⁶ F. J. G. de Abajo, *ACS Photonics* **1** (2014).
- ⁷ Y. V. Bludov, N. M. R. Peres, and M. I. Vasilevskiy, *Journal of Optics* **15**, 114004 (2013).
- ⁸ T. Stauber, *J. Phys.: Condens. Matter* **26**, 123201 (2014).
- ⁹ J. Chen, M. Badioli, P. Alonso-González, S. Thongrattanasiri, F. Huth, J. Osmond, M. Spasenović, A. Centeno, A. Pesquera, P. Godignon, et al., *Nature* **487**, 77 (2012).
- ¹⁰ Z. Fei, A. S. Rodin, G. O. Andreev, W. Bao, A. S. McLeod, M. Wagner, L. M. Zhang, Z. Zhao, M. Thiemens, G. Dominguez, et al., *Nature* **487**, 82 (2012).
- ¹¹ P. A. D. Gonçalves and N. M. R. Peres, *An Introduction to Graphene Plasmonics* (World Scientific, Singapore, 2016).
- ¹² F. H. L. Koppens, D. E. Chang, and F. J. G. de Abajo, *Nano Lett.* **11**, 3370 (2011).
- ¹³ O. L. Berman, V. S. Boyko, R. Y. Kezerashvili, A. A. Kolesnikov, and Y. E. Lozovik, *Physics Letters A* **374**, 4784 (2010).
- ¹⁴ O. L. Berman and R. Y. Kezerashvili, *Journal of Physics: Condensed Matter* **24**, 015305 (2012).
- ¹⁵ Z. Arefinia and A. Asgari, *Physica E: Low-Dimensional Systems and Nanostructures* **54**, 34 (2013), ISSN 13869477.
- ¹⁶ C. Qin, B. Wang, H. Huang, H. Long, K. Wang, and P. Lu, *Optics Express* **22**, 25324 (2014).
- ¹⁷ A. J. Chaves, N. M. R. Peres, and F. A. Pinheiro, *Phys. Rev. B* **92**, 195425 (2015).
- ¹⁸ H. Hajian, A. Soltani-Vala, and M. Kalafi, *Optics Communications* **292**, 149 (2013).
- ¹⁹ S. A. El-Naggar, *Optical and Quantum Electronics* **47**, 1627 (2015).
- ²⁰ F. Al-sheqefi and W. Belhadj, *Superlattices and Microstructures* **88**, 127 (2015).
- ²¹ A. Madani and S. R. Entezar, *Physica B: Condensed Matter* **431**, 1 (2013).
- ²² Y. H. Cheng, C. Chen, K. Y. Yu, and W. J. Hsueh, *Optics Express* **23**, 28755 (2015).
- ²³ C. S. R. Kaipa, A. B. Yakovlev, G. W. Hanson, Y. R. Padooru, F. Medina, and F. Mesa, *Physical Review B - Condensed Matter and Materials Physics* **85**, 4 (2012).
- ²⁴ Z. Xu, C. Chen, S. Q. Y. Wu, B. Wang, J. Teng, C. Zhang, and Q. Bao, *Graphene-polymer multilayer heterostructure for terahertz metamaterials* (2013).
- ²⁵ K. V. Sreekanth, S. Zeng, J. Shang, K.-T. Yong, and T. Yu, *Scientific reports* **2**, 737 (2012).
- ²⁶ Y. Fan, Z. Wei, H. Li, H. Chen, and C. M. Soukoulis, *Physical Review B* **88**, 1 (2013), 1311.7037.
- ²⁷ B. Wang, X. Zhang, F. J. García-Vidal, X. Yuan, and J. Teng, *Physical Review Letters* **109**, 1 (2012).
- ²⁸ Y. Fan, B. Wang, H. Huang, K. Wang, H. Long, and P. Lu, *Optics Letters* **39**, 6827 (2014).
- ²⁹ F. Wang, C. Qin, B. Wang, S. Ke, H. Long, K. Wang, and P. Lu, *Optics Express* **23**, 31136 (2015).
- ³⁰ Y. V. Bludov, D. A. Smirnova, Y. S. Kivshar, N. M. R. Peres, and M. I. Vasilevskiy, *Physical Review B* **91**, 045424 (2015).
- ³¹ Z. Wang, B. Wang, H. Long, K. Wang, and P. Lu, *Optics Express* **23**, 32679 (2015).
- ³² K. V. Sreekanth, S. Zeng, K. T. Yong, and T. Yu, *Sensors and Actuators, B: Chemical* **182**, 424 (2013).
- ³³ J.-T. Liu, N.-H. Liu, H. Wang, T.-B. Wang, and X.-J. Li, *Physica B: Condensed Matter* **452**, 66 (2014).
- ³⁴ B. Sensale-Rodriguez, R. Yan, M. M. Kelly, T. Fang, K. Tahy, W. S. Hwang, D. Jena, L. Liu, and H. G. Xing, *Nature communications* **3**, 780 (2012).
- ³⁵ H. Yan, X. Li, B. Chandra, G. Tulevski, Y. Wu, M. Freitag, W. Zhu, P. Avouris, and F. Xia, *Nature Nanotechnology* **7**, 330 (2012).
- ³⁶ I. V. Iorsh, I. S. Mukhin, I. V. Shadrivov, P. A. Belov, and Y. S. Kivshar, *Physical Review B* **87**, 075416 (2013).
- ³⁷ S. V. Zhukovsky, A. Andryeuskii, J. E. Sipe, and A. V. Lavrinenko, *Physical Review B* **90**, 155429 (2014).
- ³⁸ M. Cheng, P. Fu, M. Weng, X. Chen, X. Zeng, S. Feng, and R. Chen, *Journal of Physics D: Applied Physics* **48**, 285105 (2015).
- ³⁹ A. Vakil and N. Engheta, *Science (New York, N.Y.)* **332**, 1291 (2011).
- ⁴⁰ B. Rejaei and A. Khavasi, *J. of Opt.* **17**, 075002 (2015).
- ⁴¹ Y. V. Bludov, A. Ferreira, N. M. R. Peres, and M. I. Vasilevskiy, *International Journal of Modern Physics B* **27**, 1341001 (2013).
- ⁴² Here the parity is considered with respect to the middle of the dielectric slab between the graphene sheets, i.e. the plane $z = (m + 1/2) d$.
- ⁴³ L. L. Chang, L. Esaki, and R. Tsu, *Appl. Phys. Lett.* **24**, 593 (1974).